IEEE Access
Multidisciplinary | Rapid Review | Open Access Journal

Received May 3, 2022, accepted May 29, 2022, date of publication June 2, 2022, date of current version June 8, 2022.

Digital Object Identifier 10.1109/ACCESS.2022.3179700

An Indirect Type-2 Fuzzy Neural Network Optimized by the Grasshopper Algorithm for Vehicle ABS Controller

ABDOLLAH AMIRKHANI[1], (Senior Member, IEEE), MASOUD SHIRZADEH[2], (Member, IEEE), AND MAHDI MOLAIE[1]

[1]School of Automotive Engineering, Iran University of Science and Technology, Tehran 16846-13114, Iran
[2]Department of Electrical Engineering, Amirkabir University of Technology (Tehran Polytechnic), Tehran 15875-4413, Iran

Corresponding author: Abdollah Amirkhani (amirkhani@iust.ac.ir)

ABSTRACT Model nonlinearity, structured and unstructured uncertainties as well as external disturbances are some of the most important challenges in controlling the wheel slip in moving vehicles. Based on the interval type-2 fuzzy neural network, we construct an indirect exponential sliding-mode (ESM) controller for improving the performance of vehicle antilock braking systems (VABSs) in the face of the uncertainties. Lyapunov stability postulate is used to verify the stability of the closed-loop system and also to extract the adaptation rules. In this scheme, the reaching law for the sliding surface is regulated based on an exponential surface in order to eliminate the produced chattering. Selecting appropriate controller constants and adaptation rules leads to quicker signal convergence and a better management of the control signal restrictions. These constants are optimized by defining a cost function and employing the grasshopper optimization algorithm (GOA) to search for an optimal solution. Thus, we provide an optimized robust adaptive indirect ESM controller with GOA for VABS. The efficacy of the proposed method is verified by analyzing the obtained results and comparing its performance with some other control schemes for various road conditions and driving maneuvers. The results of this work affirm that the designed method makes a significant improvement in the performance of VABS control.

INDEX TERMS Interval type-2 fuzzy, neural network, antilock braking system, grasshopper optimization, sliding-mode.

I. INTRODUCTION

The existing faults and flaws in vehicle subsystems are considered to be an important cause of road accidents; and, therefore, the researchers in the automobile industry have focused their efforts on the prevention or mitigation of these problems [1]. These research endeavors have led to the development of various driver-assistance systems and active safety mechanisms in vehicles. Normally, the active safety systems are the type of mechanisms that either alert the drivers of imminent dangers or directly interfere in vehicle operations [2]. These systems help prevent or reduce the severity of road accidents by using the data they receive from the installed sensors and cameras [3]. The vehicle antilock braking system (VABS) is one of the most effective mechanisms of vehicle chassis control during hard braking [4]. The development of vehicle chassis control systems has attracted a great deal of attention in the research arenas and the automobile industry. Among these systems, the VABS is used to directly control the longitudinal dynamics of vehicles during braking. The main function of a VABS is to prevent the locking of the wheels during braking and to regulate the longitudinal wheel slip within its desired range in order to produce the maximum amount of braking force. A VABS can regulate the magnitude of the longitudinal force; so it is used in the lower layer of a vehicle's dynamic control system [5], [6]. The locking of a car's wheels during braking leads to the loss of its maneuverability in the lateral direction; as a result, the vehicle is no longer steerable and it becomes vulnerable to potential accidents and crashes [6]. In this case, a VABS uses the sensor data and checks for the locking of the wheels by monitoring the longitudinal speed of the vehicle. As soon as the tires lock, the VABS changes the braking force applied to the wheels [7].

The associate editor coordinating the review of this manuscript and approving it for publication was Wenbing Zhao.

This is exactly what a driver does in this situation by repeatedly pressing and releasing the brake pedal. However, a VABS does this at a much faster rate and is able to avoid the locking of the wheels during braking [8]. In addition to the prevention of wheels locking, another important goal of a VABS is to provide enough traction and adhesion between tires and road so that sufficient friction can be generated for stopping a vehicle [9]. Thus, a VABS plays an important role in preserving the stability and reducing the stopping distance of a vehicle during hard braking [10].

The existing nonlinearities and the uncertainties in the modeling of vehicle dynamics are two major problems afflicting the design of VABSs [9]. Model uncertainties arise from factors such as tire force saturation, variation of road surface conditions and the changes of vehicle parameters such as mass, center of gravity, etc. Also, the un-modeled or overlooked dynamics during the modeling process as well as the actual vehicle limitations are considered as the unstructured uncertainties. An effective controller for VABS should be able to successfully manage the existing uncertainties and nonlinearities in the vehicle model. To these, we should add external disturbances as well. Moreover, the control law for VABS should be such that a computed control input (e.g., brake pressure) can be easily tuned and kept to a minimum. So there seems to be a need to design a robust nonlinear VABS controller. Owing to the recent technological advancements, the performance of a VABS can be greatly enhanced [11]. Among the different control techniques developed so far, the sliding mode control (SMC) is considered to be an effective method. This technique has been studied extensively; and, due to its simplicity and robustness, it is now used in many industrial applications [12]. An integral SMC based wheel slip regulation has been proposed in [13] to exploit the responsiveness of regenerative brakes during braking. Some other approaches that employ the SMC for VABS control include the method of gray system modeling for SMC [14], fractional order SMC [15], time-varied SMC [16], and the adaptive fractional order SMC [17]. Some other VABS control methods include the nonlinear solutions [18], data-driven approaches [19], adaptive nonlinear controllers [20], and the enhanced nonlinear predictive strategy [21]. In addition to the techniques mentioned here, there are intelligent VABS control methods such as the fuzzy logic system (FLS) [22], neural networks (NNs) [23] and fuzzy NNs (FNNs) [8]. FLSs and NNs are two types of approximators with excellent performances. The NN approximator and the T1-FLS approximator have been used in [24], [25], respectively. The combination of FLSs and NNs for the approximation of nonlinear functions has yielded good results [26]. The performance of a NN approximator is enhanced by adding the FLS. The combination of T1-FNN and wavelet, as an approximator, has been used in [26], [27].

The introduction of the FLS theory helped enhance the ability of different systems in confronting various uncertainties [28]. There are two types of FLS: type-1 (T1) FLS, and type-2 (T2) FLS [29]. In the T1-FLS, an uncertainty is expressed by an exact number in the range of (0, 1) as interpreted as a degree of membership function [30]. The T2-FLS, which uses a T2 fuzzy set (FS), was proposed to deal with the limitations of T1-FLS [31]. The T2-FLSs are divided into two categories of interval T2 (IT2) FLSs and general T2 (GT2) FLSs [32]. Nowadays, the T2-FLSs (whether IT2-FLSs or GT2-FLSs) are employed in numerous areas such as medical diagnosis [33], security monitoring and control [34], transportation applications [35], design of electronic commerce services [36], and robot control [37]. Regarding the use of FLS in VABS control, we can mention the following works. A T1-FLS for VABS control was presented in [38], which estimates the tire-road friction coefficient and vehicle speed by using the recursive least square approximation method. A proportional-integral-derivative controller based on genetic T1-FLS was presented in [39]. To verify the performance of an open-loop T1-FLS based method, a software test was performed in [22]. In this approach, the T1-FLS acts simultaneously as a controller and road surface estimator. Considering the variations of road conditions, a T1-FLS has been presented in [40], and to minimize the number of simulations related to T1-FLS, an optimization method based on genetic algorithm (GA) has been proposed in this work. Besides the FLSs, the NNs constitute another family of supervised learning models that mimic the human central nervous system. Owing to their ability to learn from input-output data, NNs are extensively employed in many applications, including control engineering [41]–[46]. Based on the capabilities of NNs, a predictive method for VABS control is presented in [9] and an adaptive VABS controller is devised in [23]. The manual tuning of the FLS parameters can be a tedious and time-consuming task if we intend to achieve the desired results. As a possible solution to this problem, it has been suggested to combine the NNs with the FLSs. These hybrid methods simultaneously benefit from the ability of the FLSs in dealing with uncertainties and the learning capability of the NNs. These combinations have led to the development of hybrid methods such as T1-FNN [47] and T2-FNN [37].

As was previously mentioned, although the SMC is a simple and robust technique, it suffers from a chattering problem [48], [49]. In order to reduce the amount of chattering, we can approximate the sign function (SF) [44], [50]. However, the approximation of SF leads to error and ensures only a uniformly ultimately bounded system stability in this case [50]. To reduce the error caused by the approximation of SF, the gain of the SF can be determined by using the FLS [30], [51]. This method is employed in conjunction with the T1-FLS for controlling the VABS [52], [53]. Although using the FLS (either T1 or T2) to obtain the SMC gain reduces the approximation error, mathematically, the problem still remains.

Another problem about the works on SMC applications, especially those on vehicle and VABS control, is that these methods are not optimized. One solution is to use the evolutionary algorithms for optimizing these techniques. The

grasshopper optimization algorithm (GOA) [54] imitates the natural searching behavior and the social interactions of grasshoppers. Following its introduction, the GOA has been employed in many different applications [55]. Therefore, we can use the GOA as an appropriate algorithm for optimizing the control methods. In view of the problems associated with the use of the SMC technique on VABS, and also with regards to the nonlinearities and uncertainties related to vehicle dynamics, road condition variations, changes of vehicle parameters, and external disturbances, a robust and adaptive VABS method has been presented in this paper by employing an exponential sliding-mode (ESM) and IT2-FNN. In this approach, the IT2-FNN parameters are updated online and the problems associated with the conventional SMC method are alleviated by using an exponential reaching law. Not only is the proposed controller stable, but also the size of the generated control signals can be managed and they can be made to converge faster by selecting proper constants for the controller. The optimal values for these constants were selected by defining an appropriate cost function and using the GOA. In other words, a robust ESM-IT2 fuzzy adaptive neural (FAN) method optimized by the GOA has been presented in this work for controlling the VABS. A review of the literature shows that because of the system nonlinearity, parametric uncertainties and the disturbances applied to a vehicle, the subject of tire slip control in VABSs is still a challenging issue. Moreover, only a few studies are conducted on the adaptive robust fuzzy control of wheel slip in VABSs by considering the parametric and un-modeled uncertainties. These have been the motivations for proposing a fuzzy robust adaptive controller in this paper. The innovations of the proposed scheme and the contributions of the presented work are as follows:

- The proposed scheme assumes that the system dynamics are unknown and that they can get upset by random disturbances such as varying road conditions and vehicle parameters.
- The unidentified and disturbed dynamics of VABS are approximated online by means of an IT2-FAN. This reduces the volume of the computations and enables the real-time implementation of the proposed technique.
- The robustness of the proposed method against the external disturbances and varying road surface conditions is guaranteed.
- By using an exponential sliding manifold along with a FAN, the global and un-chattered asymptotic convergence of system dynamics in the control signal and the approximation of the sign function are guaranteed.
- Heuristic algorithms are used to determine the constant parameters of the IT2-FAN and ESM.
- By evaluating the proposed technique simultaneously via the CarSim and Matlab, the simulation environment is brought closer realistic conditions.

The rest of this paper has been organized as follows. The formulation of the problem, including the mathematical formulas of the car model, tires, and other parts, is presented in Section 2. The IT2-FNN is briefly reviewed in Section 3. The ESM-IT2-FAN method and its proof of stability are presented in Section 4. The optimization of the devised method by means of the GOA is carried out in Section 5. Section 6 presents the optimization results and compares the performances of the proposed technique with the other methods in terms of controlling the vehicle's motion under different maneuvers and driving conditions. Finally, the conclusion of the work is presented in Section 7.

II. PROBLEM FORMULATION

The following vehicle model equations are used to develop the wheel slip controller [23], [40], [53]:

$$F_x + M_t \dot{v}_x = 0 \tag{1}$$

$$\tau_b = R_w F_x + \tau_d - I_w \dot{\omega} \tag{2}$$

$$\lambda = 1 - \frac{R_w \omega}{v_x} \tag{3}$$

$$M_t = 0.25 m_{vs} + m_w \tag{4}$$

where, v_x is the vehicle longitudinal velocity, F_x is the longitudinal braking force, ω is the angular velocity, $I_w$is the wheel moment of inertia, R_w is the wheel radius, τ_b is the braking torque, τ_d is disturbance, $\lambda$is the wheel slip during braking, m_{vs} is the vehicle sprung mass and m_w is the wheel mass. The normal load of tire is expressed as

$$F_z = m_t g - \frac{m_{vs} h_{cg}}{2 l_w} \ddot{x} \tag{5}$$

where l_w is the distance between two axles, g is the gravitational acceleration, $\ddot{x}$ is the longitudinal acceleration and h_{cg} is the height of the vehicle sprung mass. The normal tire load (F_z) is actually computed by measuring the longitudinal acceleration $\ddot{x}$; however, in simulation studies, F_z is calculated by inserting Eq. (1) into Eq. (5) and numerically solving the resulting nonlinear equation. The modified Dugoff model has been used for modeling the longitudinal braking force. This model is expressed as follows [49], [56]:

$$\begin{aligned} F_x &= c_x \lambda \Gamma f(\varpi) h_x \\ F_y &= c_y \Gamma \tan\alpha f(\varpi) h_y \end{aligned} \tag{6}$$

$$f(\varpi) = \begin{cases} \varpi(2 - \varpi) & \varpi \le 1 \\ 1 & \varpi > 1 \end{cases} \tag{7}$$

$$\varpi = \frac{\mu F_z \left(1 - \varepsilon_r v \sqrt{\lambda^2 + \tan(\alpha)}\right)}{2\Gamma \sqrt{c_x^2 \lambda^2 + c_y^2 \tan^2(\alpha)}} \tag{8}$$

$$\Gamma = (1 - \lambda)^{-1} \tag{9}$$

where, c_x and c_y indicate the tire stiffness, αdenotes the side slip angle of tires, μ represents the road friction factor and ε_r is the road adhesion reduction coefficient. Also, h_x, h_y and $\mu(\lambda)$ are written as

$$h_x = (1.15 - 0.75\mu)\lambda^2 - (1.63 - 0.75\mu)\lambda + 1.5 \tag{10}$$

$$h_y = (\mu - 1.6)\tan(\alpha) + 1.5 \tag{11}$$

$$\mu = \vartheta_1 \sin\{\vartheta_2 \arctan[\vartheta_3\lambda - \vartheta_4(\vartheta_3\lambda - \arctan(\vartheta_3\lambda))]\} \tag{12}$$

In (12), $\vartheta_i, i = 1, \ldots, 4$ are the parameters of the friction model, which depend on the road conditions. By differentiating (3) and substituting (1) and (2) into it, we will have

$$\dot{\lambda} = \underbrace{-\frac{1}{v_x}\left(\frac{R_w}{I_w}F_x + \frac{F_x}{M}(1-\lambda)\right)}_{f(\mathbf{x})} + \underbrace{\frac{R_w}{I_w v_x}}_{g(\mathbf{x})}\tau_b \underbrace{-\frac{R_w}{I_w v_x}}_{T_d}\tau_d \tag{13}$$

If we consider $\mathbf{x} = (v_x, \lambda)^T$ as a state vector, the dynamic equation for the derivative of wheel slip during braking will be obtained as

$$\dot{\lambda} = f(\mathbf{x}) + g(\mathbf{x})\tau_b + T_d(t) \tag{14}$$

By assuming the external disturbance to be bounded (i.e., $|T_d| \leq \Upsilon_1$), then $\Upsilon_1 \in \Re_+$ will be the upper bound for the external disturbance, where $\Re_+$ is a set of real positive numbers.

III. INTERVAL TYPE-2 FUZZY NEURAL NETWORK

An IT2-FNN is a nonlinear system with inputs $\boldsymbol{\chi} = (\chi_1, \ldots, \chi_{N_i}) \in \Re^{N_i}$ and outputs $y_o = f(\boldsymbol{\chi}) \in \Re^{N_o}$. In general, an IT2-FNN includes N_i inputs and N_o outputs. The overall form of the rules for an IT2-FLS is as follows [31], [37], [57]:

$$R^{k_i}: \text{if} x_1 \text{is}_1\tilde{A}_j^{k_i} \text{and} x_2 \text{is}_2\tilde{A}_j^{k_i} \cdots x_{N_i} \text{is}_{N_i}\tilde{A}_j^{k_i} \text{ then } Y^{k_i} = W^{k_i} k_i = 1, 2, \ldots, N_r, j = 1, 2, .., N_m \tag{15}$$

The k_i^{th} rule has been presented in (15), in which N_r indicates the number of rules, $N_m$is the number of membership functions, and $\left\{{}_1\tilde{A}_j^{k_i}, {}_2\tilde{A}_j^{k_i}, \ldots, {}_{N_1}\tilde{A}_j^{k_i}\right\}$ represent the IT2-FSs. In the consequent section of the rules, Y^{k_i} designates a number in the interval $W^{k_i} = \left[w^{k_i}, \bar{w}^{k_i}\right]$. $w^{k_i} = \left(w_1^{k_i}, \ldots, w_{N_o}^{k_i}\right)$ and $\bar{w}^{k_i} = \left(\bar{w}_1^{k_i}, \ldots, \bar{w}_{N_o}^{k_i}\right)$ are the lower and upper bounds of this interval, respectively. The structure of the proposed IT2-FNN has 5 layers. In the first layer (input layer), there are neurons whose number is equal to the number of inputs. The fuzzifier is in the second layer. In this layer, the non-fuzzy inputs are converted to fuzzy numbers by means of IT2-FSs. Every IT2-FS has an upper and a lower bound, and the distance between the upper and lower bounds is known as the footprint of uncertainty. An IT2-FS is defines as [58]:

$$\bar{\mu}_{{}_kA_j^{k_i}} = \begin{cases} {}^1\mu_{{}_kA_j^{k_i}}, & x_i < {}_k^1b_j^{k_i} \\ 1, {}_k^1b_j^{k_i} \leq x_i \leq {}_k^2b_j^{k_i} \\ {}^2\mu_{{}_kA_j^{k_i}}, & x_i > {}_k^2b_j^{k_i} \end{cases}$$

$$\mu_{{}_kA_j^{k_i}} = \begin{cases} {}^2\mu_{{}_kA_j^{k_i}}, & x_i \leq 0.5\left({}_k^1b_j^{k_i} + {}_k^2b_j^{k_i}\right) \\ {}^1\mu_{{}_kA_j^{k_i}}, & x_i > 0.5\left({}_k^1b_j^{k_i} + {}_k^2b_j^{k_i}\right) \end{cases} \tag{16}$$

In (16), x_i is the i^{th} input. Also, ${}^1\mu_{{}_kA_j^{k_i}}$ and ${}^2\mu_{{}_kA_j^{k_i}}$ indicate the degrees of membership of two T1-FS. A T1-FS is expressed as

$${}^1\mu_{{}_kA_j^{k_i}} = \exp\left(-\frac{1}{2}\left(\frac{x_i - {}_k^1b_j^{k_i}}{{}_k\sigma_j^{k_i}}\right)^2\right), {}^2\mu_{{}_kA_j^{k_i}} = \exp\left(-\frac{1}{2}\left(\frac{x_i - {}_k^2b_j^{k_i}}{{}_k\sigma_j^{k_i}}\right)^2\right) \tag{17}$$

where ${}_k\sigma_j^{k_i}$ is the standard deviation (STD), and ${}_k^1b_j^{k_i}$ and ${}_k^2b_j^{k_i}$ are the centers of Gaussian functions. In the third layer, which is the inference layer, the t-norm is used for inferencing. The output of this layer is defined as:

$$\left[z_l^{k_i}(\boldsymbol{\chi}), z_r^{k_i}(\boldsymbol{\chi})\right] = \begin{bmatrix} \mu_{{}_1A_j^{k_i}}(x_1) \cap \cdots \cap \mu_{{}_{N_i}A_j^{k_i}}(x_{N_i}), \\ \bar{\mu}_{{}_1A_j^{k_i}}(x_1) \cap \cdots \cap \bar{\mu}_{{}_{N_i}A_j^{k_i}}(x_{N_i}) \end{bmatrix} \tag{18}$$

In (18), $\cap$ designates the sign of the t-norm. We use the multiplication t-norm for the inferencing process. In the fourth layer, the Enhanced Karnik-Mendel (EKM) type-reducer is employed to convert an IT2-FS into a T1-FS [59]. The outputs of the fourth layer are as follows [37], [58], [60]:

$$y_r^{k_o} = = \frac{\sum_{k_i=1}^{R} z_l^{k_i}\bar{w}_k^{k_i} + \sum_{k_i=R+1}^{N_r} z_r^{k_i}\bar{w}_k^{k_i}}{\sum_{k_i=1}^{R} z_l^{k_i} + \sum_{j=R+1}^{N_r} z_r^{k_i}} = \bar{w}_k^T\bar{\boldsymbol{\xi}} \tag{19}$$

$$y_l^{k_o} = \frac{\sum_{k_i=1}^{L} z_r^{k_i}w_k^{k_i} + \sum_{k_i=L+1}^{N_r} z_l^{k_i}w_k^{k_i}}{\sum_{k_i=1}^{L} z_r^{k_i} + \sum_{k_i=L+1}^{N_r} z_l^{k_i}} = w_k^T\boldsymbol{\xi} \tag{20}$$

In the above equations, L and R are obtained by means of the EKM algorithm. Also, $\bar{\boldsymbol{\xi}}$ and $\boldsymbol{\xi}$ are defined as

$$\bar{\boldsymbol{\xi}} = \frac{1}{\sum_{k_i=1}^{R} z_l^{k_i} + \sum_{k_i=R+1}^{N_r} z_r^{k_i}}\left(z_l^1, \ldots, z_l^R, z_r^{R+1}, \ldots, z_r^{N_r}\right)^T$$

$$\boldsymbol{\xi} = \frac{1}{\sum_{k_i=1}^{L} z_r^{k_i} + \sum_{k_i=L+1}^{N_r} z_l^{k_i}}\left(z_r^1, \ldots, z_l^L, z_l^{L+1}, \ldots, z_l^{N_r}\right)^T \tag{21}$$

The fifth layer of the proposed IT2-FNN is the output layer. The k_o^{th} output of the IT2-FNN will be

$$y^{k_o} = 0.5\left(y_r^{k_o} + y_l^{k_o}\right) \tag{22}$$

In vector form, the output of the IT2-FNN is obtained as

$$\mathbf{Y} = 0.5(Y_l + Y_r) = \mathbf{w}^{\mathbf{T}}\boldsymbol{\xi} \tag{23}$$

where $Y_l = \mathbf{w}^{\mathbf{T}}\boldsymbol{\xi}$, $Y_r = \bar{\mathbf{w}}^{\mathbf{T}}\bar{\boldsymbol{\xi}}$ and $\boldsymbol{\xi} = 0.5\left(\boldsymbol{\xi}^T\ \bar{\boldsymbol{\xi}}^T\right)^T$. Also, the matrixes $\mathbf{w}$ and $\bar{\mathbf{w}}$ are expressed as

$$\mathbf{w} = \begin{pmatrix} w_1^1 & w_{N_o}^1 \\ w_1^{N_r} & w_{N_o}^{N_r} \end{pmatrix}, \bar{\mathbf{w}} = \begin{pmatrix} \bar{w}_1^1 & \bar{w}_{N_o}^1 \\ \bar{w}_1^{N_r} & \bar{w}_{N_o}^{N_r} \end{pmatrix} \tag{24}$$

By considering the fuzzy systems approximation theory, the IT2-FNN can be employed to approximate an unknown function [61].

IV. EXPONENTIAL SLIDING-MODE INTERVAL TYPE-2 FUZZY ADAPTIVE NEURAL CONTROLLER

Eq. (14) can be written as

$$\dot{\lambda} = \bar{f}(\mathbf{x}) + \bar{g}(\mathbf{x})\tau_b + T_d(t) + H \tag{25}$$

where $H = \Delta f(\mathbf{x}) + \Delta g(\mathbf{x})\tau_b$, $f(\mathbf{x}) = \bar{f}(\mathbf{x}) + \Delta f(\mathbf{x})$ and $g(\mathbf{x}) = \bar{g}(\mathbf{x}) + \Delta g(\mathbf{x})$. $\bar{f}(\mathbf{x})$ and $\bar{g}(\mathbf{x})$ respectively indicate the values of $f(\mathbf{x})$ and $g(\mathbf{x})$ without the uncertainty. The values of $\bar{f}(\mathbf{x})$ and $\bar{g}(\mathbf{x})$ are known, but H has an unknown value. Suppose $|H| \leq \Upsilon_2$ and $\Upsilon_2 \in \Re_+$. The sliding surface is defined as

$$s = e(t) + \beta \int e(t')\, dt' \tag{26}$$

where $e(t) = \lambda - \lambda_d$ is the error, λ_d is the reference slip which should be tracked by the wheel slip, and $\beta \in \Re_+$ is a constant parameter. We differentiate the sliding surface and substitute (13) instead of $\dot{\lambda}$.

$$\dot{s} = \bar{f}(\mathbf{x}) + \bar{g}(\mathbf{x})\tau_b + T_d(t) + H - \dot{\lambda}_d + \beta e \tag{27}$$

If $\dot{s}$ is equated to zero, the equivalent control signal will be obtained as

$$\tau_b = (\bar{g}(\mathbf{x}))^{-1}\left(\dot{\lambda}_d - \beta e - \bar{f}(\mathbf{x}) - T_d(t) - H\right) \tag{28}$$

The value of H is not actually available. The unknown function H is approximated by means of the IT2-FNN. Also, here, any disturbance is bounded. The ideal parameters of $\Delta\hat{H}(\mathbf{x})$ are expressed as

$$\mathbf{w}_H^* = \arg\min\left[\sup_{\mathbf{x}\in\mathbf{U_x}}\left|\hat{H}(\mathbf{x}|\mathbf{w}_H) - H(\mathbf{x})\right|\right] \tag{29}$$

In (29), $\hat{H}(\mathbf{x})$ is the approximation of $H(\mathbf{x})$ and $\mathbf{U_x}$ indicates the range of $\mathbf{x}$. By applying the Taylor expansion, the difference between the value estimated by the IT2-FNN and the optimal approximated function is obtained as follows:

$$\hat{H}(\mathbf{x}|\mathbf{w}_H) - \hat{H}\left(\mathbf{x}|\mathbf{w}_H^*\right) = \left(\mathbf{w}_H - \mathbf{w}_H^*\right)^T\left(\frac{\partial\hat{H}(\mathbf{x}|\mathbf{w}_H)}{\partial\mathbf{w}_H}\right) + h.o.t\left(\left|\mathbf{w}_H - \mathbf{w}_H^*\right|^2\right) \tag{30}$$

In (30), $h.o.t\left(\left|\mathbf{w}_H - \mathbf{w}_H^*\right|^2\right)$ signifies the higher-order terms. Furthermore, the function approximated by the IT2-FNN can be defined by the expression $\mathbf{w}_H^T\boldsymbol{\xi}_H(\mathbf{x})$ and by using the approximation error of ε_H. If we assume ε_H to be bounded ($|\varepsilon_H| \leq \Upsilon_3$), $\Upsilon_4 \in \Re_+$will be the upper bound for the approximation error.

$$\hat{H}(\mathbf{x}|\mathbf{w}_H) = \mathbf{w}_H^T\boldsymbol{\xi}_H + \varepsilon_H \tag{31}$$

In (31), $\boldsymbol{\xi}_H = {\partial\hat{H}(\mathbf{x}|\mathbf{w}_H)}/{\partial\mathbf{w}_H}$. The difference between the value of the optimized function and the value estimated by the IT2-FNN is obtained as

$$\begin{aligned}\hat{H}^*\left(\mathbf{x}|\mathbf{w}_H^*\right) - \hat{H}(\mathbf{x}|\mathbf{w}_H) &= \left(\mathbf{w}_H^* - \mathbf{w}_H\right)^T\boldsymbol{\xi}_H + \varepsilon_H \\ &= \tilde{\mathbf{w}}_H^T\boldsymbol{\xi}_H + \varepsilon_H\end{aligned} \tag{32}$$

Due to the presence of approximation error and disturbance, a compensator (u_c) is added to the control signal to ensure the stability of the closed-loop system.

$$\tau_b = \hat{\tau}_{eq} + \tau_c = \underbrace{(\bar{g}(\mathbf{x}))^{-1}\left(\dot{\lambda}_d - \beta e - \bar{f}(\mathbf{x}) - \hat{H}(\mathbf{x}|\mathbf{w}_H)\right)}_{\hat{\tau}_{eq}} + (\bar{g}(\mathbf{x}))^{-1}u_c \tag{33}$$

The control signal and the optimal approximated function are inserted into the Eq. (27).

$$\dot{s} = \tilde{\mathbf{w}}_H^T\boldsymbol{\xi}_H + \varepsilon_H + T_d(t) + u_c \tag{34}$$

A Lyapunov function is considered as

$$L = 0.5\left(s^2 + \gamma_H^{-1}\tilde{\mathbf{w}}_H^{\mathbf{T}}\tilde{\mathbf{w}}_H\right) \tag{35}$$

where $\gamma_H \in \Re_+$ denotes the adaptation rate. We take the derivative of Eq. (35) and substitute (34) into this derivative.

$$\begin{aligned}\dot{L} &= s\dot{s} + \gamma_H^{-1}\tilde{\mathbf{w}}_H^{\mathbf{T}}\dot{\mathbf{w}}_H \\ &= s\tilde{\mathbf{w}}_H^T\boldsymbol{\xi}_H + s\varepsilon_H + sT_d + su_c - \gamma_H^{-1}\tilde{\mathbf{w}}_H^{\mathbf{T}}\dot{\mathbf{w}}_H \\ &= s\varepsilon_H + sT_d + su_c + \tilde{\mathbf{w}}_H^T\left(s\boldsymbol{\xi}_H - \gamma_H^{-1}\dot{\mathbf{w}}_H\right)\end{aligned} \tag{36}$$

The adaptation rules for the IT2-FNN parameters are designed as follows:

$$\dot{\mathbf{w}}_H = \gamma_H s\boldsymbol{\xi}_H \tag{37}$$

Thus, (36) is simplified as

$$\dot{L} = s\varepsilon_H + sT_d + su_c \tag{38}$$

Parameter u_c is defined as

$$u_c = -(\delta_4 + (1-\delta_4)\exp(-\delta_2|s|))^{-1}(\delta_1\mathrm{sgn}(s) + \delta_3 s) \tag{39}$$

where $\delta_i\,(i = 1, 2, 3) \in \Re_+$ and $0 < \delta_4 < 1$ are constant parameters and $\mathrm{sgn}(\bullet)$ designates a SF. Now we substitute (39) into (38).

$$\begin{aligned}\dot{L} &= s\varepsilon_H + sT_d \\ &\quad + s\left(-(\delta_4 + (1-\delta_4)\exp(-\delta_2|s|))^{-1}(\delta_1\mathrm{sng}(s) + \delta_3 s)\right) \\ &= s\varepsilon_H + sT_d - (\delta_4 + (1-\delta_4)\exp(-\delta_2|s|))^{-1}\left(\delta_1|s| + \delta_3 s^2\right) \\ &\leq |s||\varepsilon_H| + |s||T_d| - (\delta_4 + (1-\delta_4)\exp(-\delta_2|s|))^{-1} \\ &\quad \times\left(\delta_1|s| + \delta_3 s^2\right) \\ &\leq |s|\Upsilon_3 + |s|\Upsilon_1 - (\delta_4 + (1-\delta_4)\exp(-\delta_2|s|))^{-1} \\ &\quad \times\left(\delta_1|s| + \delta_3 s^2\right)\end{aligned} \tag{40}$$

The value of $\exp(-\delta_2|s|)$ is between 0 and 1; which results in the following equations:

$$\begin{aligned}\delta_4 &\leq \delta_4 + (1-\delta_4)\exp(-\delta_2|s|) \\ &\leq \delta_4 + (1-\delta_4) \\ (\delta_4 + (1-\delta_4))^{-1} &\leq (\delta_4 + (1-\delta_4)\exp(-\delta_2|s|))^{-1} \leq \delta_4^{-1} \\ -\delta_4^{-1} &\leq -(\delta_4 + (1-\delta_4)\exp(-\delta_2|s|))^{-1} \\ &\leq -(\delta_4 + (1-\delta_4))^{-1}\end{aligned} \tag{41}$$

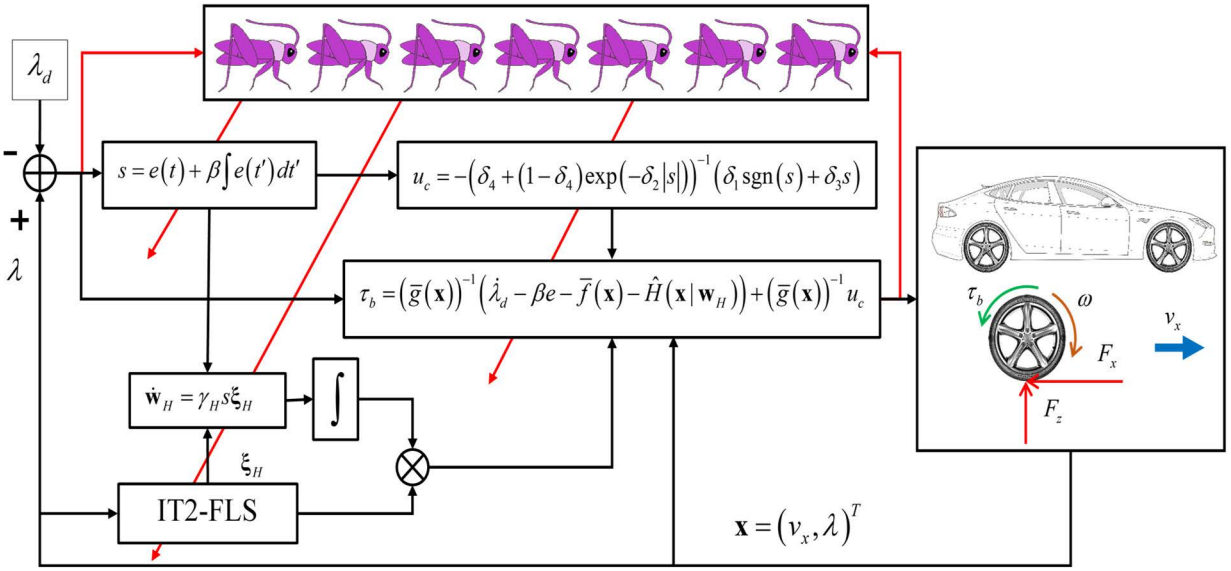

FIGURE 1. The structure of the ESM-IT2-FNN controller optimized by the GOA.

In view of (41), and if $\Upsilon = \Upsilon_1 + \Upsilon_3 < \delta_1 (\delta_4 + (1 - \delta_4))^{-1}$, the derivative of the Lyapunov function will be negative.

$$\begin{aligned}\dot{L} &\leq |s|\,\Upsilon - (\delta_4 + (1-\delta_4)\exp(-\delta_2|s|))^{-1}\left(\delta_1|s| + \delta_3 s^2\right)\\ &\leq |s|\,\Upsilon - (\delta_4 + (1-\delta_4))^{-1}\left(\delta_1|s| + \delta_3 s^2\right)\\ &= |s|\,\Upsilon - \delta_1 (\delta_4 + (1-\delta_4))^{-1}|s| - \delta_3 (\delta_4 + (1-\delta_4))^{-1} s^2\\ &= -\left(\delta_1 (\delta_4 + (1-\delta_4))^{-1} - \Upsilon\right)|s|\\ &\quad - \delta_3 (\delta_4 + (1-\delta_4))^{-1} s^2 \leq 0 \end{aligned} \tag{42}$$

So, $\tilde{\mathbf{w}}_H$ will have finite values. If we define B as follows:

$$\begin{aligned}B = \int_0^t \Big(&-\left(\delta_1 (\delta_4 + (1-\delta_4))^{-1} - \Upsilon\right)|s|\\ &- \delta_3 (\delta_4 + (1-\delta_4))^{-1} s^2\Big)\, dt' \end{aligned} \tag{43}$$

B will satisfy the conditions of Barbalat's lemma [50]. With the elapse of time,$\dot{B} \to 0$ and, therefore, s will approach zero as well. Thus, the closed-loop system will be stable. Fig. 1 shows the structure of the ESM-IT2-FAN method optimized by the GOA. This figure also displays the forces applied to the car wheel. In the next section, we present the GOA and describe how the proposed controller is optimized.

V. CONTROLLER OPTIMIZATION

An important aspect of designing a robust adaptive controller is to identify appropriate constants for the adaptation rules obtained. In addition to system stability, the faster convergence of the algorithm and the restriction of the control signal are also important issues, which are ignored in many of the studies on robust and adaptive control techniques. To investigate this subject in the present work, the following cost function has been considered so as to minimize the system error as quickly as possible despite the saturation of control inputs.

$$\begin{aligned}&\min F_c(\tau_b, e, t) = \left(\int_0^{t_f} (\alpha_1 t\,|e| + \alpha_2\,|\Delta\tau_b|)\, dt\right)\\ &\text{Subjected to: } |\tau_b| \leq \tau_{\max},\ \delta_i\ (i = 1, \ldots, 3) \in \Re_+,\\ &\qquad 0 < \delta_4 < 1,\\ &\qquad \beta, \gamma_H, {}_k\sigma_j^{k_i} \in \Re_+, \quad -1 < {}_k^1 b_j^{k_i}, {}_k^2 b_j^{k_i} < 1 \end{aligned} \tag{44}$$

In (44), $\Delta\tau_b$ represents the variations of control signal and $\tau_{\max}$ indicates the maximum control signal. $\alpha_1, \alpha_2 \in \Re_+$ are constant parameters, and t_f is the simulation finish time. The above optimization problem is solved by applying the GOA. The behavior of a group of grasshoppers can be considered as follows [54]:

$$\begin{aligned}&P_i^g(n+1)\\ &= S_i^g(n) + G_i^g(n) + w_i^g(n)\ i = 1, \ldots, N_{pop}, n = 1, \ldots, n_M \end{aligned} \tag{45}$$

In (45), N_{pop} is the total number of grasshopper populations, n is the number of iterations, n_M is the maximum iteration, $P_i^g(n)$ is the position of the i$^{\text{th}}$ grasshopper, $S_i^g(n)$ is the social interaction of the i$^{\text{th}}$ grasshopper, $G_i^g(n)$ is the force of gravity on the i$^{\text{th}}$ grasshopper, and $w_i^g(n)$ is the wind effect on the i$^{\text{th}}$ grasshopper. The social interaction between grasshoppers is defined as

$$S_i^g = \sum_{j=1(j\neq i)}^{N_{pop}} s_p(d_{ij}) \frac{P_j^g - P_i^g}{d_{ij}} \tag{46}$$

where $d_{ij} = \left|P_j^g - P_i^g\right|$ is the Euclidean distance between the ith and jth grasshoppers. $s_p(\bullet)$ is a function that shows the strength (intensity) of the social forces and is expressed as

$$s_p\left(d_{ij}\right) = a_I \exp\left(\frac{-d_{ij}}{a_L}\right) - \exp\left(-d_{ij}\right) \tag{47}$$

In (47), a_I and a_L respectively denote the attraction intensity and the attraction length scale. Parameter $s_p(\bullet)$ indicates the effects of the social interactions (attraction and repulsion) of grasshoppers.

The distance values (d_{ij}) in this function are mapped into the interval [1, 4]. Eq. (45) is for modeling the behavior of grasshoppers in the outdoors and it is not suitable for optimization. To be able to use this modeling for optimization and also to enable the algorithm to properly explore and exploit the search space for a solution, this formula is modified as follows [55]:

$${}^dP_i^g = \eta\left(\sum_{j=1(j\neq i)}^{N_{pop}} \eta\frac{ub_d - lb_d}{2} s\left(\left|{}^dP_i^g - {}^dP_j^g\right|\right)\frac{P_i - P_j}{d_{ij}}\right) + {}^d\hat{P}_B \tag{48}$$

In the modified formula, ub_d and lb_d are the upper and lower bounds in the d^{th} dimension, respectively, and ${}^d\hat{P}_B$ is the best solution found (up to the iteration n) in the d^{th} dimension. The constant parameter η is used to both control the exploration and exploitation activities in the search space and also to manage the areas of attraction, neutrality, and repulsion between the grasshoppers [55]. Parameter η is considered as

$$\eta = \eta_{\min} + \left(1 - \left(\frac{n}{n_M}\right)^{\rho}\right)^{1/\rho}(\eta_{\max} - \eta_{\min}) \tag{49}$$

$\eta_{\min}$ and $\eta_{\max}$ indicate the minimum and maximum values of η ($\eta_{\min} \leq \eta \leq \eta_{\max}$), respectively, and ρ is a constant parameter which should be tuned. At the start of the algorithm execution, η has a large value (exploration receives a large share), which gradually diminishes as the number of iterations goes up. Here, the parameters associated with the ESM-IT2-FAN are used to establish the grasshopper population.

VI. RESEARCH FINDINGS

The numerical parameters used in the simulation are presented in Table 1. One of the problems associated with designing a controller for the existing subsystems in autonomous vehicles is the changes that occur in those numerical parameters. These fluctuations have been considered as parametric uncertainties and incorporated into the problem formulation according to Table 1. Controller design and optimization is done based on the nominal parameters. The simulations were performed on a PC with 12 GB of RAM and Core i7 processor with 3.5 GHz frequency in the MATLAB (v. 2018a).

A constant time step of 0.001 s was considered in the Simulink. The velocity of the wheels during braking is almost zero; so, wheel slip approaches infinity. The simulation is terminated when the car velocity is about 5 m/s. IT2-FNN is used for the online detection of the nonlinear function of H. The IT2-FNN inputs for the detection of these function is (v_x, λ).

TABLE 1. The value of parameters.

Parameter	Nominal Value	Time<=1.5s	1.5s<Time<=3s	3s<Time	Unit
m_w	45	45	58.5	63	kg
m_{vs}	1460	1460	1898	2044	kg
h_{cg}	0.385	0.385	0.385	0.385	m
l_w	2.87	2.87	3.731	4.018	m
g	9.81	9.81	9.81	9.81	m/s
R_w	0.336	0.336	0.4368	0.4704	m
I_w	1.85	1.85	2.405	2.59	kg.m^2
c_x	50000	50000	65000	70000	N/unit slip
c_y	20000	20000	20000	20000	N/rad
ε_r	0.015	0.015	0.015	0.015	s/m
α	0	0	0	0	rad
α_1	1	-	-	-	-
α_2	0.001	-	-	-	-

A. OPTIMIZATION RESULTS

The optimization results obtained by using the GOA, particle swarm optimization (PSO) and GA have been reported in Table 2. By varying the parameters of the optimization algorithms, the performances of the GOA in an ESM-IT2-FAN VABS controller are evaluated and compared in Table 2. The statistical analysis of the optimization results is also performed in Table 2, as follows. In each row of this table, the parameters of an optimization algorithm are randomly changed within a specific range. The optimization process for each of these parameters is repeated 10 times. In PSO, w_I is the weight inertia, φ_1 is the personal learning coefficient and φ_2 is the global learning coefficient.

The mean and the STD values of the cost function for these iterations are listed in Table 2 in the relevant columns.

This table also provides the mean NFE (number of cost function evaluation) values, the average simulation times (STs) and best cost function (BCF). Mean and STD values have also been displayed graphically in Fig. 2 as box plots. In the optimization procedures, the initial vehicle velocity and wheel slip are considered as $v_x(0) = (30 + 5\text{rand})\,m/s$ and $\lambda(0) = 0$, respectively; where "rand" indicates a random number which causes a different initial velocity to be used every time the simulation is rerun.

To illustrate the effect of the GOA on the IT2-FSs, the results obtained for these IT2-FSs in several iterations of the GOA are plotted in Fig. 3. In order to have a graphical display and comparison of GOA convergence in addition to the statistical analysis provided, the graphs of the cost function versus the NFE values for several optimization algorithms are

TABLE 2. The results of the ESM-IT2-FAN controller with different optimization algorithms.

GOA												
Figure	n	N_{pop}	$\eta_{\min}$	$\eta_{\max}$	ρ	a_I	a_L	**ST(s)**	**NFE**	**BCF**	**Mean**	**STD**
-	5	5	1e-5	1.0	0.6	0.5	1.5	929	30	0.00198710	0.00462513	0.00052914
-	10	10	1e-5	1.0	0.6	0.5	1.5	4389	110	0.00128900	0.00168631	0.00031287
-	15	15	1e-5	1.0	0.6	0.5	1.5	10954	240	0.00091029	0.00175346	0.00039570
Fig. 2(a)	20	20	1e-5	1.0	0.6	0.5	1.5	13912	420	0.00083122	0.00172243	0.00016249
-	5	5	1e-4	1.0	0.7	0.6	1.4	820	30	0.00141163	0.00239797	0.00045834
-	10	10	1e-4	1.0	0.7	0.6	1.4	4650	110	0.00103124	0.00261447	0.00013320
-	15	15	1e-4	1.0	0.7	0.6	1.4	8253	240	0.00093620	0.00138138	0.00011415
Fig. 2(b)	20	20	1e-4	1.0	0.7	0.6	1.4	18965	420	0.00083496	0.00181657	0.00013824
-	5	5	1e-6	1.5	0.7	0.5	1.5	781	30	0.00124953	0.00277065	0.00017781
-	10	10	1e-6	1.5	0.7	0.5	1.5	5590	110	0.00097508	0.00116486	0.00009414
-	15	15	1e-6	1.5	0.7	0.5	1.5	9339	240	0.00090008	0.00177801	0.00012225
Fig. 2(c)	20	20	1e-6	1.5	0.7	0.5	1.5	21066	420	0.00896322	0.00187555	0.00004113
Fig. 2(d)	20	10	1e-6	1.5	0.7	0.5	1.5	10416	210	0.00096010	0.00215425	0.00019292
-	10	5	1e-3	1.0	0.6	0.4	1.5	1580	55	0.00112361	0.00213574	0.00016953
-	10	10	1e-5	1.0	0.5	0.4	1.6	3846	110	0.00087766	0.00111609	0.00017425
-	10	15	1e-6	1.5	0.8	0.6	1.3	5841	165	0.00074157	0.00125250	0.00010149
Fig. 2(e)	10	15	1e-5	1.0	0.7	0.4	1.7	5692	165	0.00089983	0.00187708	0.00010653
Fig. 2(f)	15	20	1e-4	1.0	0.9	0.6	1.4	11594	320	0.00087895	0.00191013	0.00010663
PSO												
Figure	n	N_{pop}	φ_1	φ_2	w_I	**ST(s)**	**NFE**	**BCF**	**Mean**	**STD**		
-	5	5	2.05	2.05	1.00	991	30	0.00198710	0.00418531	0.00056249		
-	10	10	2.05	2.05	1.00	4228	110	0.00128900	0.00265243	0.00035244		
-	15	15	2.05	2.05	1.00	10214	240	0.00091029	0.00189227	0.00029244		
Fig. 2(a)	20	20	2.05	2.05	1.00	17813	420	0.00084156	0.00171657	0.00022537		
-	5	5	1.67	1.67	1.00	862	30	0.00141400	0.00288236	0.00041415		
-	10	10	1.67	1.67	1.00	4996	110	0.00103220	0.00213417	0.00014043		
-	15	15	1.67	1.67	1.00	8903	240	0.00093881	0.00199947	0.00011793		
Fig. 2(b)	20	20	1.67	1.67	1.00	16919	420	0.00093406	0.00191657	0.00016824		
-	5	5	2.05	1.67	1.00	778	30	0.00116860	0.00234846	0.00017271		
-	10	10	1.67	2.05	1.00	5263	110	0.00096977	0.00197622	9.8461e-05		
-	15	15	1.67	2.05	1.00	9525	240	0.00093881	0.00194254	0.00011793		
Fig. 2(c)	20	20	2.05	1.67	1.00	21290	420	0.00094452	0.00191657	0.00005582		
Fig. 2(d)	20	10	1.67	2.05	1.00	10182	210	0.00106100	0.00211657	0.00011152		
-	10	5	2.05	1.67	0.90	1892	55	0.00117990	0.00213636	0.00016081		
-	10	10	1.87	1.12	0.95	3759	110	0.00095179	0.00197724	0.00017514		
-	10	15	1.97	1.98	0.95	5979	165	0.00080594	0.00161460	0.00010221		
Fig. 2(e)	10	15	0.99	1.64	0.14	5925	165	0.00094697	0.00191427	0.00011306		
Fig. 2(f)	15	20	0.86	1.87	0.79	12717	320	0.00092956	0.00191657	0.00011924		
GA												
Figure	n	N_{pop}	**Crossover**	**Mutation**	**ST(s)**	**NFE**	**BCF**	**Mean**	**STD**			
-	5	5	0.80	0.20	1177	30	0.00234370	0.00473681	0.0013865			
-	10	10	0.80	0.20	5829	110	0.00171040	0.00346163	0.00030435			
-	15	15	0.80	0.20	12392	240	0.00093121	0.00199758	0.00014327			
Fig. 2(a)	20	20	0.80	0.20	22656	420	0.00088758	0.00186239	0.00016584			
-	5	5	0.74	0.26	1503	30	0.00175840	0.00358711	0.0011024			
-	10	10	0.74	0.26	6491	110	0.00108860	0.00229778	0.00048598			
-	15	15	0.74	0.26	13611	240	0.00124830	0.00253289	0.00056486			
Fig. 2(b)	20	20	0.74	0.26	21555	420	0.00087191	0.00176239	8.8262e-05			
-	5	5	0.28	0.72	1427	30	0.00271532	0.00475135	0.00004721			
-	10	10	0.62	0.38	5484	110	0.00153270	0.00316144	0.00043649			
-	15	15	0.40	0.60	7717	240	0.00137360	0.00271618	0.00059717			
Fig. 2(c)	20	20	0.45	0.55	14450	420	0.00092296	0.00186239	0.00012415			
Fig. 2(d)	20	10	0.54	0.46	12252	210	0.00106391	0.00216239	0.00022784			
-	10	5	0.69	0.31	2791	55	0.00304330	0.00618823	0.0013103			
-	10	10	0.75	0.25	5775	110	0.00227140	0.00458104	0.0015156			
-	10	15	0.67	0.33	10005	165	0.00120960	0.00242755	0.00063455			
Fig. 2(e)	10	15	0.72	0.28	4748	165	0.00155570	0.00316239	0.00048628			
Fig. 2(f)	15	20	0.67	0.33	17685	320	0.00089720	0.00186239	0.00021631			

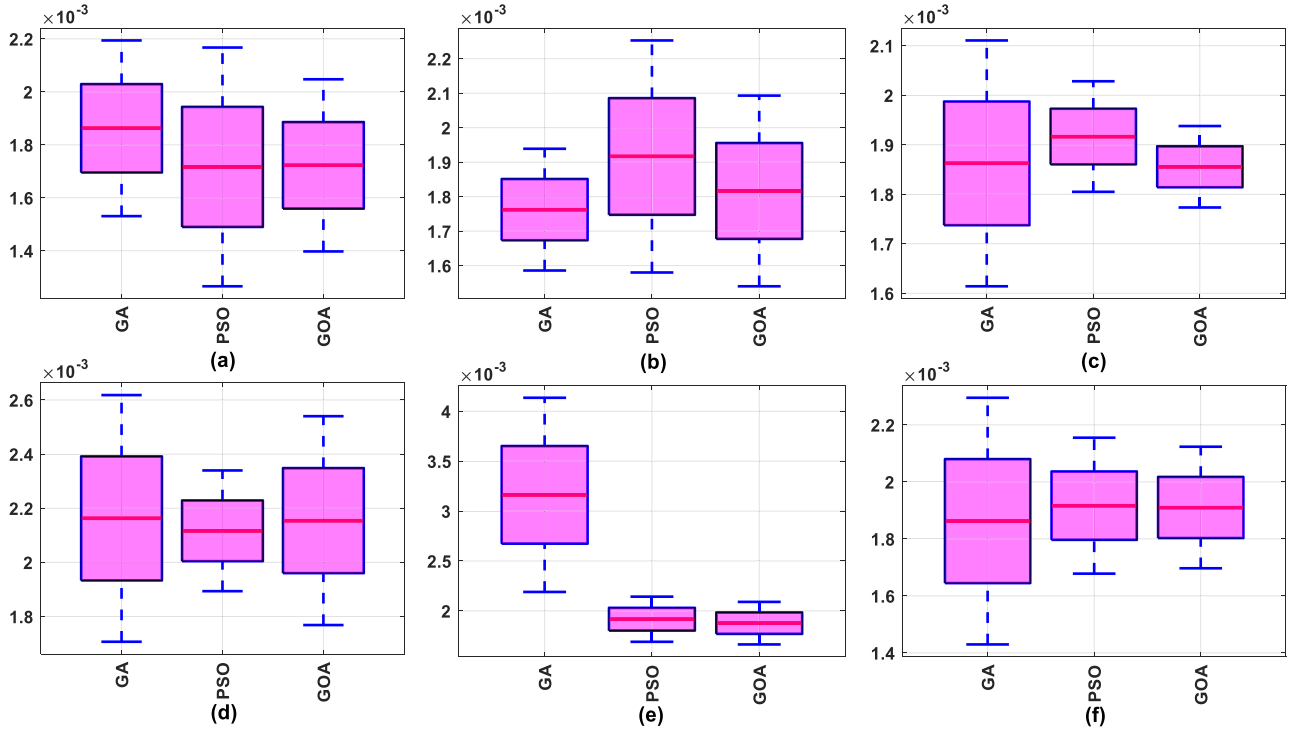

FIGURE 2. The statistical analysis results for different optimization algorithms.

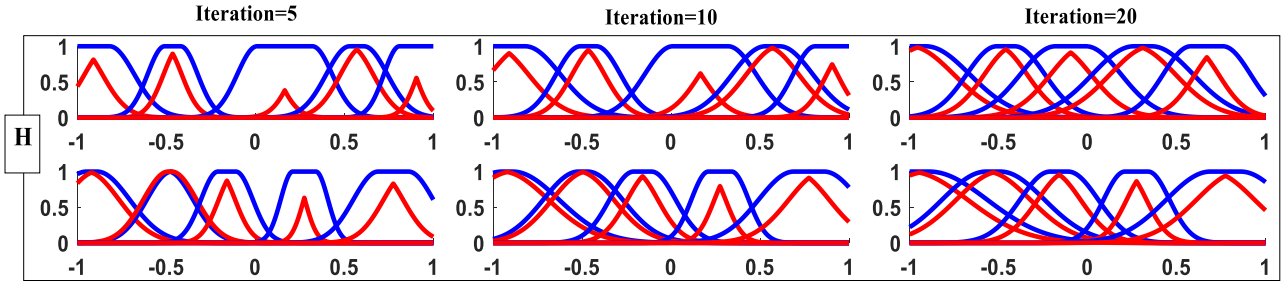

FIGURE 3. The variations of IT2-FS in several iterations of the GOA.

presented in Fig. 4. The initial vehicle speed and wheel slip in this case are $v_x(0) = 30$m/s and $\lambda(0) = 0$, respectively. In addition to Fig. 4, the convergence results of GOA are presented in Fig. 5. This figure shows the graphs of cost function values versus the number of iterations in different conditions. As is observed, after several iterations, the cost function converges to a fixed value.

Different factors determine the complexity and the volume of computations of the GOA. The average run times for the GOA had been previously presented in Table 2. For a deeper evaluation of this factor, the graphs of the average execution times for the GOA as well as the maximum iteration values versus the numbers of grasshopper populations have been plotted in Fig. 6. Also, by looking at the GOA, we can say that $NFE = N_{pop}\,(n_M + 1)$.

B. CONTROLLER RESULTS

The parameters of the proposed ESM-IT2-FAN controller optimized by the GOA are listed in Table 3. To evaluate the robustness and the performance of this controller, different maneuvers were designed and analyzed. In the first maneuver, in the absence of any disturbance, uncertainty and control signal saturation, a moving vehicle brakes on a dry road ($\vartheta_1 = 0.9$, $\vartheta_2 = 2.1$, $\vartheta_3 = 5$ and $\vartheta_4 = 0.98$).

Fig. 7, shows the vehicle speed, wheel slip error, and control input (braking torque). According to this figure, the wheel slip is able to successfully track the reference value and the error approaches zero. Also, the control signal is devoid of chattering.

In the second maneuver, the road surface changes drastically during braking operations. These conditions are

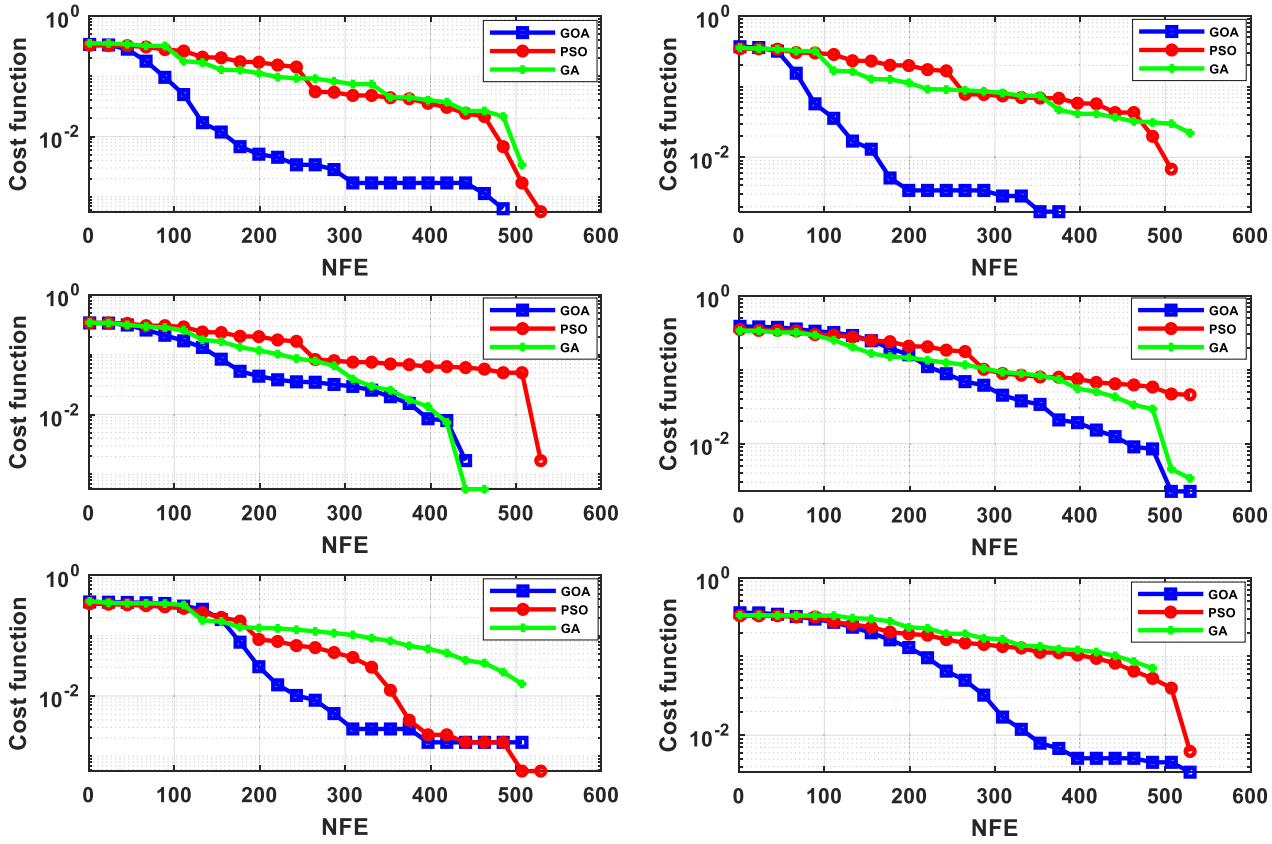

FIGURE 4. Cost function values versus NFE of various optimization algorithms.

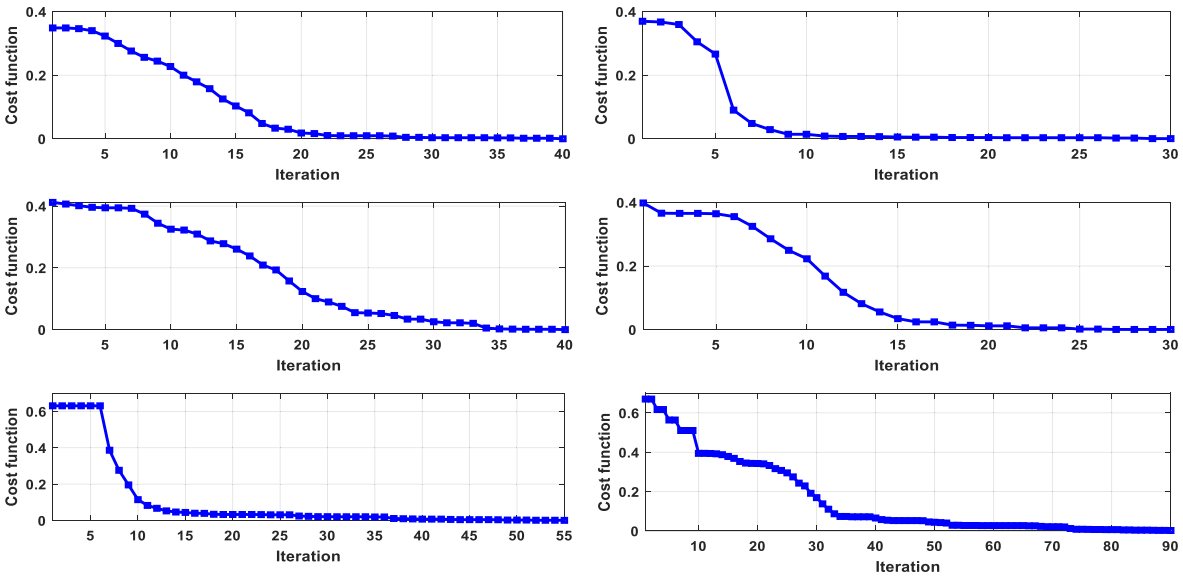

FIGURE 5. Cost function values versus the number of iterations in different conditions.

reflected in the simulation by changing the value of the friction model parameters. Changes in road conditions in terms of braking distance are presented in Table 4. We show the brake distance with d_x. The results of this maneuver

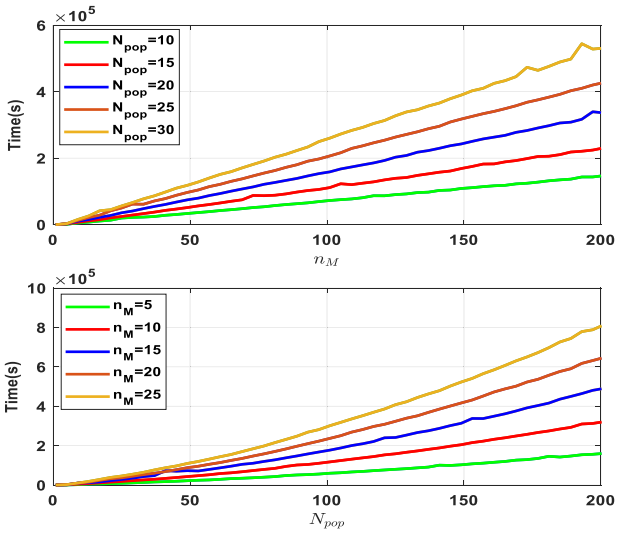

FIGURE 6. The average execution times for the GOA as well as the maximum iteration values versus the numbers of grasshopper populations.

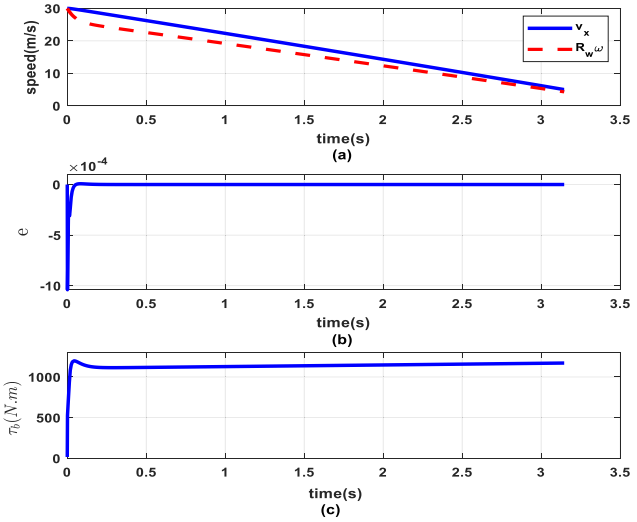

FIGURE 7. The results of the first maneuver; (a) vehicle angular velocity, (b) wheel slip error, and (c) braking torque.

are illustrated in Fig. 8. According to Fig. 8(a), despite the severe changes of the road surface conditions, the wheel slip error ha approached zero. For a visual comparison with other methods, the results of an ESM-T1-FAN controller have also been presented in Fig. 8.

In the third maneuver, we investigate the effects of parametric uncertainties in the modeling. In this case, besides the severe changes of road surface conditions, some uncertainties in vehicle parameters (according to Table 1) are also taken into consideration. The results of the proposed ESM-IT2-FAN controller and of the ESM-T1-FAN controller for the third maneuver are presented simultaneously in Fig. 9.

In the fourth maneuver, in addition to the road surface changes and the parametric uncertainties, an external disturbance is added to the system. In this maneuver, a maximum saturation limit of $\tau_{\max} = 1200$N.m is also considered for the control signal. Fig. 10 shows the results of this maneuver, including the wheel slip error and the braking torque. In addition to the results of the proposed ESM-IT2-FAN controller, the results of the ESM-T1-FAN controller have also been illustrated in Fig. 10.

The results of these maneuvers indicate that: firstly, the control signals of both considered methods are without chattering (Figs. 8(b), 9(b) and 10(b)); secondly, error convergence to zero (in the presence of uncertainty, disturbance and control signal saturation) (Figs. 8(a), 9(a) and 10(a)); thirdly, the proposed ESM-IT2-FAN controller has a more desirable performance both in terms of a lower wheel slip error and a smaller control signal.

To test the method from a practical point of view, we used Matlab and CarSim. Fig. 11 shows the results of the joint simulation. The results confirm the practicality of the proposed method. According to Fig. 11, the ESM-IT2-FAN has a shorter braking distance and braking time and shows good braking performance.

TABLE 3. The controller parameters.

Parameter	Value	Parameter	Value	Parameter	Value
β	448.70	γ_H	467.52	N_m	5
N_r	5	δ_1	71.76	δ_2	292
δ_3	27.98	δ_4	0.031	${}_1^1b_1^1$	-1.00
${}_1^1b_2^2$	-0.51	${}_1^1b_3^3$	-0.18	${}_1^1b_4^4$	0.26
${}_1^1b_5^5$	0.58	${}_2^1b_1^1$	-1.00	${}_2^1b_2^2$	-0.57
${}_2^1b_3^3$	-0.21	${}_2^1b_4^4$	0.21	${}_2^1b_5^5$	0.69
${}_1^2b_1^1$	-0.91	${}_1^2b_2^2$	-0.41	${}_1^2b_3^3$	-0.01
${}_1^2b_4^4$	0.36	${}_1^2b_5^5$	0.76	${}_2^2b_1^1$	-0.89
${}_2^2b_2^2$	-0.49	${}_2^2b_3^3$	-0.11	${}_2^2b_4^4$	0.34
${}_2^2b_5^5$	0.86	${}_1\sigma_1^1$	0.35	${}_1\sigma_2^2$	0.24
${}_1\sigma_3^3$	0.28	${}_1\sigma_4^4$	0.33	${}_1\sigma_5^5$	0.22
${}_2\sigma_1^1$	0.46	${}_2\sigma_2^2$	0.35	${}_2\sigma_3^3$	0.24
${}_2\sigma_4^4$	0.17	${}_2\sigma_5^5$	0.35	-	-

TABLE 4. Changes in road conditions in terms of braking distance.

Parameters	$d_x \le 24m$	$24m < d_x \le 47m$	$47m \le d_x$
ϑ_1	0.9	0.5	0.7
ϑ_2	2.1	2.1	1.9
ϑ_3	5	4.0	4.7
ϑ_4	0.98	0.8	0.86

In order to compare the performance criteria quantitatively, we consider the measures of integral squared error (ISE), integral absolute error (IAE), integral time square error (ITSE), and integral time absolute error (ITAE). These performance criteria are defined as follows:

$$ISE = \int_0^{t_f} e^2(t)\,dt \tag{50}$$

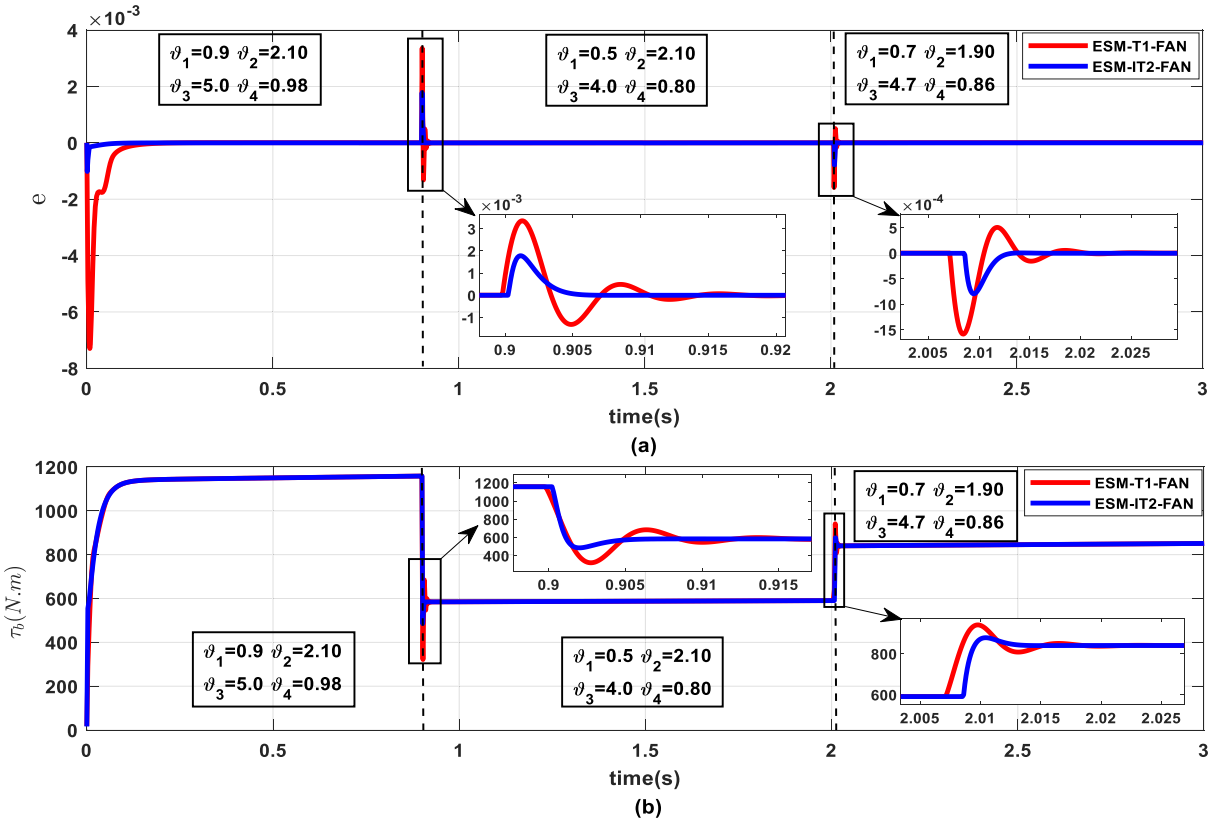

FIGURE 8. The results of the second maneuver; (a) wheel slip error, and (b) braking torque.

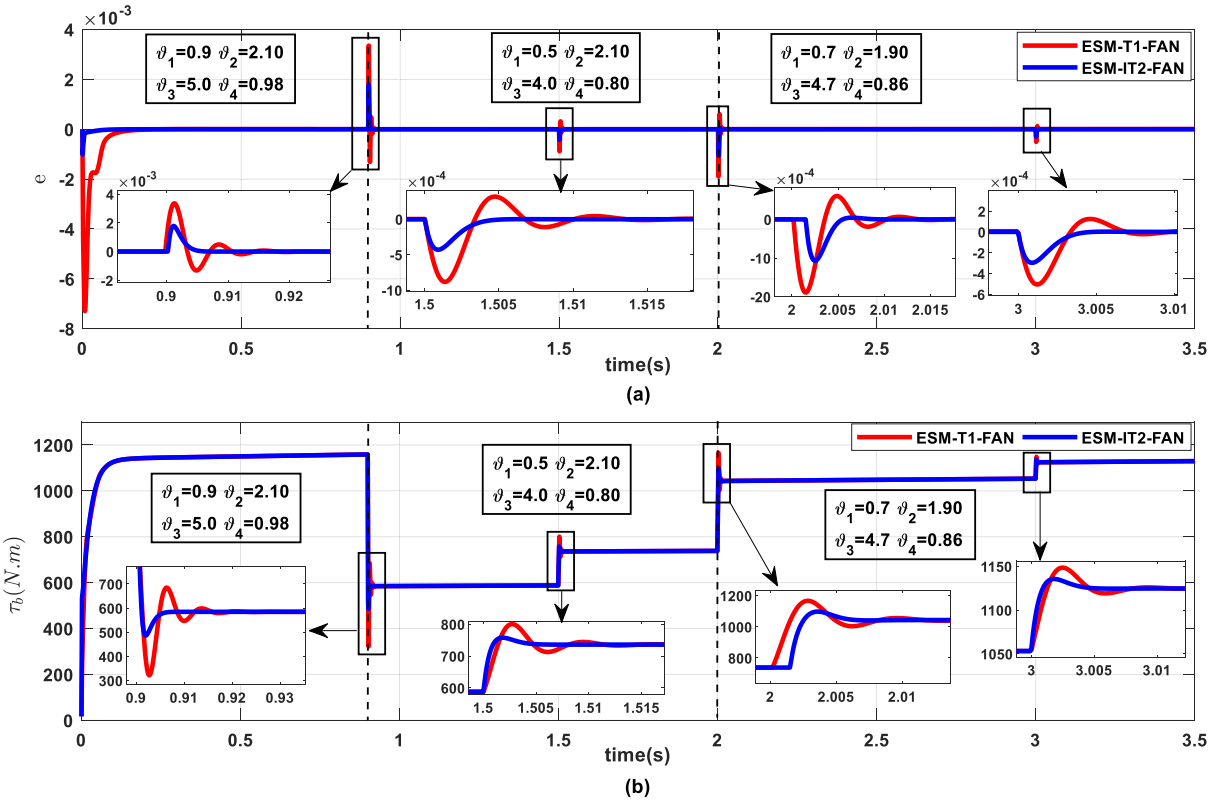

FIGURE 9. The results of the third maneuver; (a) wheel slip error, and (b) braking torque.

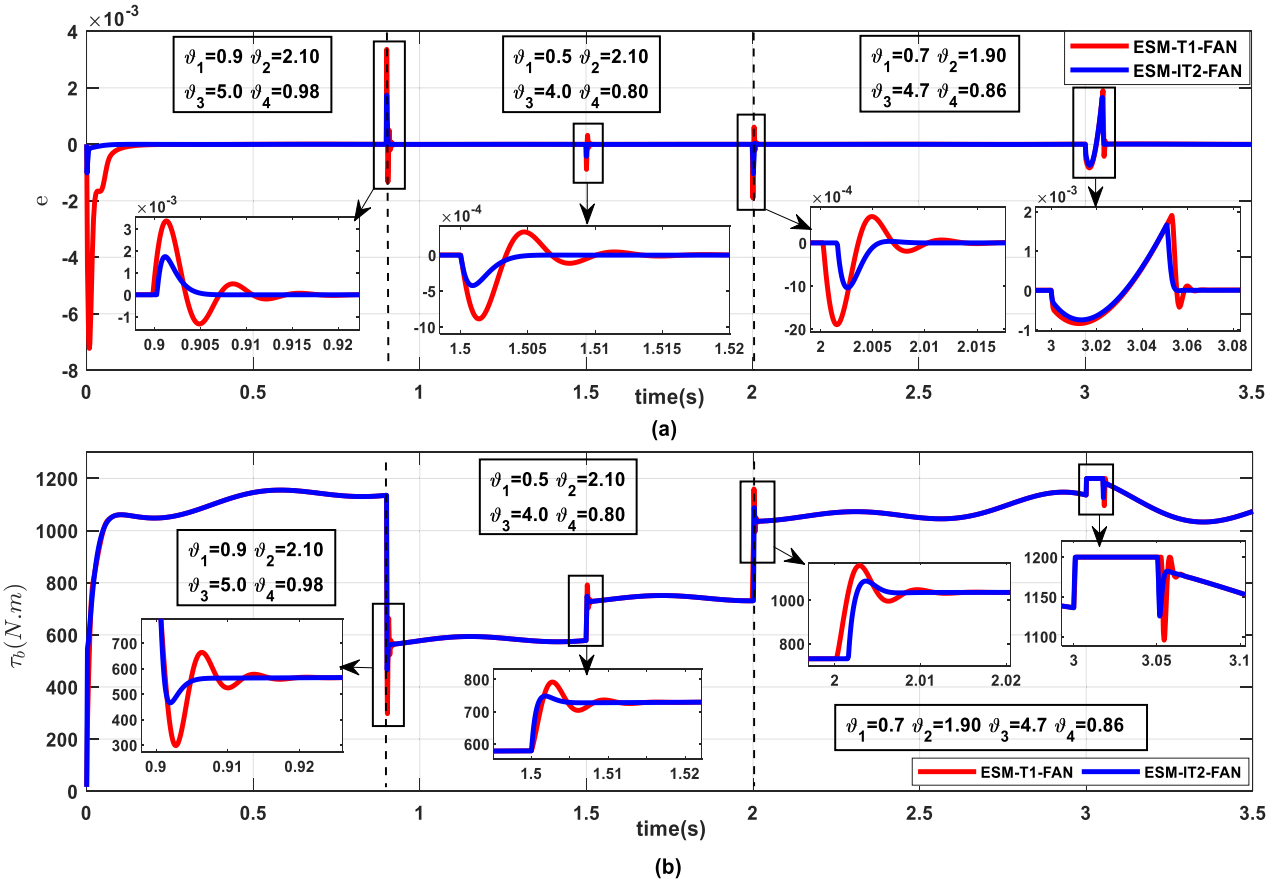

FIGURE 10. The results of the fourth maneuver; (a) wheel slip error, and (b) braking torque.

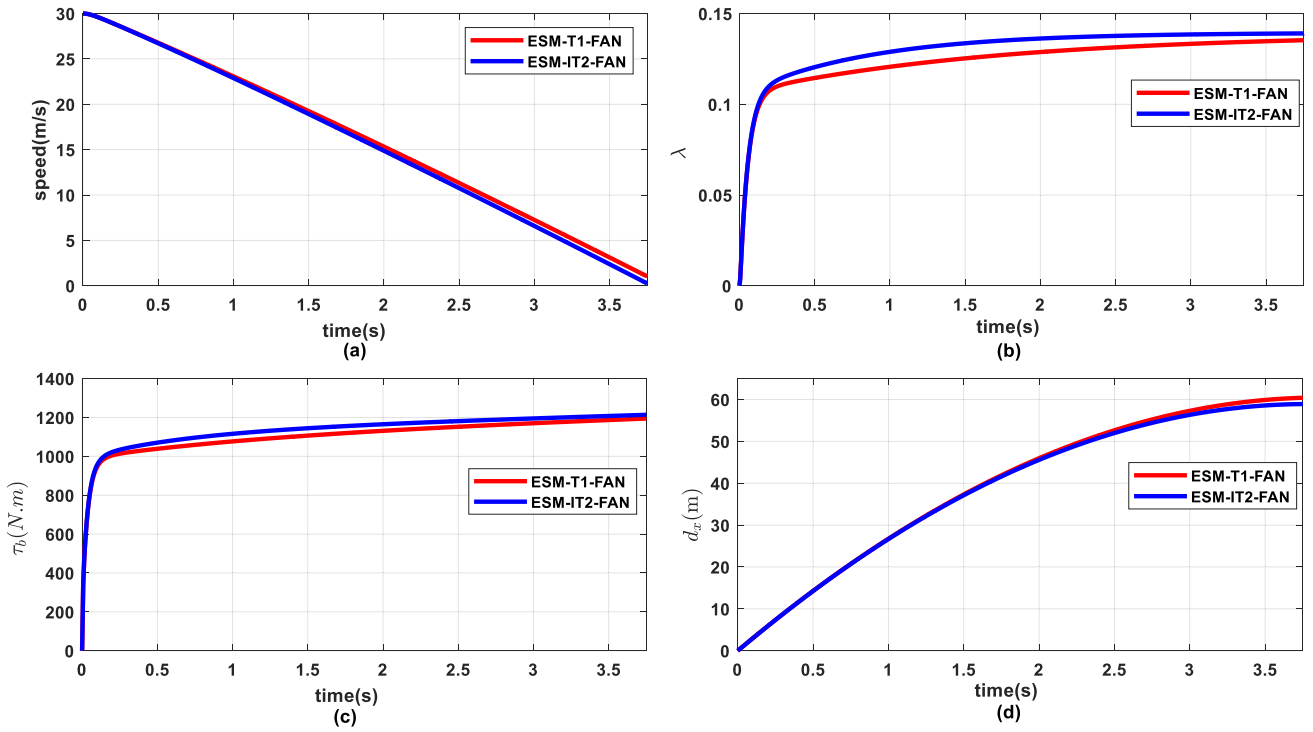

FIGURE 11. The results of the ESM-IT2-FAN and ESM-T1-FAN; (a) speed, (b) wheel slip (c) braking torque, and (d) braking distance.

TABLE 5. Quantitative comparison of controller performances in different maneuvers.

Maneuver	Performance Criteria	ESM-T1-FAN	ESM-IT2-FAN
Maneuver-I	*ISE*	7.435e-7	2.899e-9
	IAE	2.295e-4	9.446e-6
	ITSE	1.211e-8	1.633e-11
	ITAE	7.923e-5	6.093e-7
	d_x	54.65(m)	54.60(m)
	Max($\lvert\tau_b\rvert$)	1205.5(N.m)	1205.3(N.m)
Maneuver-II	*ISE*	7.712e-7	8.766e-9
	IAE	2.475e-4	1.631e-5
	ITSE	4.232e-8	6.348e-9
	ITAE	1.321e-4	1.064e-5
	d_x	74.53(m)	73.47(m)
	Max($\lvert\tau_b\rvert$)	1158.6(N.m)	1158.6 (N.m)
Maneuver-III	*ISE*	7.748e-7	1.002e-8
	IAE	2.519e-4	1.827e-5
	ITSE	4.933e-8	8.847e-9
	ITAE	1.590e-4	1.479e-5
	d_x	86.67(m)	85.59(m)
	Max($\lvert\tau_b\rvert$)	1166.4(N.m)	1158.6(N.m)
Maneuver-IV	*ISE*	7.858e-7	3.757e-8
	IAE	2.810e-4	5.602e-5
	ITSE	1.633e-7	9.338e-8
	ITAE	2.689e-4	1.304 e-4
	d_x	86.67(m)	85.59(m)
	Max($\lvert\tau_b\rvert$)	1200(N.m)	1200(N.m)

$$IAE = \int_0^{t_f} |e(t)|\, dt \tag{51}$$

$$ITSE = \int_0^{t_f} \left(e^2(t)\, t\right) dt \tag{52}$$

$$ITAE = \int_0^{t_f} (|e(t)|\, t)\, dt \tag{53}$$

The performance indexes for all the considered maneuvers are presented in Table 5. In addition to these performance criteria, the maximum braking torque values have also been given in this table.

Table 5 confirms the results presented in Figs. 8-11. Although both methods perform adequately, especially under un-ideal conditions, in controlling the wheel slip, the adaptive ESM-IT2-FAN controller achieves better results.

VII. CONCLUSION

In this paper, we have dealt with the problem of vehicle antilock braking system (VABS) control from two perspectives. First, by exploiting the capability of the interval type-2 (IT2) fuzzy neural networks, we have attempted to approximate the nonlinear functions and external disturbance online. Second, by employing an exponential sliding-mode (ESM), we have tried to compensate the effects of the approximation errors and other disturbing factors. By using an exponential reaching law, the problems associated with chattering and the errors resulting from the approximation of sign function, which exist in the common sliding methods, could be eliminated.

In this work, first we presented the mathematical formulas for VABS along with the mathematical tire model. Then a robust adaptive VABS controller was designed and the stability of the proposed method was verified by means of the Lyapunov approach. Besides the system stability, the faster convergence of the grasshopper optimization algorithm (GOA) and the restriction of the control signal are also important issues. To incorporate these features into the designed controller, a cost function was defined and the GOA was employed to search for optimal constant parameters for the controller. Eventually, a robust ESM-IT2 fuzzy adaptive neural (FAN) method optimized by the GOA was presented for VABS control. Simulation results were compared with those of the other methods developed based on the genetic algorithm and the particle swarm optimization technique. Also, a statistical analysis was performed and the computational complexity of the GOA in optimizing the proposed robust ESM-IT2-FAN controller was determined. The developed controller was then tested for VABS control in various road surface conditions and driving maneuvers. The results indicated a more effective performance of the proposed controller in different scenarios. The most important subject to consider in future research is to incorporate the dynamics of the actuators into the systems studied. Also, in the upcoming works, we intend to implement the proposed scheme on an actual system and to analyze realistic data.

REFERENCES

[1] V. K. Kukkala, J. Tunnell, S. Pasricha, and T. Bradley, "Advanced driver-assistance systems: A path toward autonomous vehicles," *IEEE Consum. Electron. Mag.*, vol. 7, no. 5, pp. 18–25, Sep. 2018.

[2] A. H. Ahangarnejad, A. Radmehr, and M. Ahmadian, "A review of vehicle active safety control methods: From antilock brakes to semiautonomy," *J. Vibrat. Control*, vol. 27, nos. 15–16, pp. 1683–1712, Aug. 2021.

[3] C. M. Martinez, M. Heucke, F.-Y. Wang, B. Gao, and D. Cao, "Driving style recognition for intelligent vehicle control and advanced driver assistance: A survey," *IEEE Trans. Intell. Transp. Syst.*, vol. 19, no. 3, pp. 666–676, Mar. 2017.

[4] X. Chen, L. Wei, X. Wang, L. Li, Q. Wu, and L. Xiao, "Hierarchical cooperative control of anti-lock braking and energy regeneration for electromechanical brake-by-wire system," *Mech. Syst. Signal Process.*, vol. 159, Oct. 2021, Art. no. 107796.

[5] M. Mirzaei and H. Mirzaeinejad, "Optimal design of a non-linear controller for anti-lock braking system," *Transp. Res. Part C: Emerg. Technol.*, vol. 24, pp. 19–35, Oct. 2012.

[6] A. T. Van Zanten, R. Erhardt, K. Landesfeind, and G. Pfaff, "VDC systems development and perspective," *SAE Trans.*, vol. 107, pp. 424–444, Jan. 1998.

[7] A. Karamoozian, H. Jiang, and C. A. Tan, "Probability based survey of braking system: A Pareto-optimal approach," *IEEE Access*, vol. 8, pp. 128385–128406, 2020.

[8] C.-M. Lin and T.-L. Le, "PSO-self-organizing interval type-2 fuzzy neural network for antilock braking systems," *Int. J. Fuzzy Syst.*, vol. 19, no. 5, pp. 1362–1374, 2017.

[9] H. Mirzaeinejad, "Robust predictive control of wheel slip in antilock braking systems based on radial basis function neural network," *Appl. Soft Comput.*, vol. 70, pp. 318–329, Sep. 2018.

[10] A. Aksjonov, V. Vodovozov, K. Augsburg, and E. Petlenkov, "Design of regenerative anti-lock braking system controller for 4 in-wheel-motor drive electric vehicle with road surface estimation," *Int. J. Automot. Technol.*, vol. 19, no. 4, pp. 727–742, Aug. 2018.

[11] F. Pretagostini, L. Ferranti, G. Berardo, V. Ivanov, and B. Shyrokau, "Survey on wheel slip control design strategies, evaluation and application to antilock braking systems," *IEEE Access*, vol. 8, pp. 10951–10970, 2020.
[12] W. Zhou, Y. Wang, and Y. Liang, "Sliding mode control for networked control systems: A brief survey," *ISA Trans.*, vol. 124, pp. 249–259, May 2022, doi: 10.1016/j.isatra.2020.12.049.
[13] K. V. Subramaniyam and S. C. Subramanian, "Electrified vehicle wheel slip control using responsiveness of regenerative braking," *IEEE Trans. Veh. Technol.*, vol. 70, no. 4, pp. 3208–3217, Apr. 2021.
[14] E. Kayacan, Y. Oniz, and O. Kaynak, "A grey system modeling approach for sliding-mode control of antilock braking system," *IEEE Trans. Ind. Electron.*, vol. 56, no. 8, pp. 3244–3252, Aug. 2009.
[15] Y. Tang, X. Zhang, D. Zhang, G. Zhao, and X. Guan, "Fractional order sliding mode controller design for antilock braking systems," *Neurocomputing*, vol. 111, pp. 122–130, Jul. 2013.
[16] S. Rajendran, S. Spurgeon, G. Tsampardoukas, and R. Hampson, "Time-varying sliding mode control for ABS control of an electric car," *IFAC-PapersOnLine*, vol. 50, no. 1, pp. 8490–8495, 2017.
[17] S. S. Moosapour, S. B. F. Asl, and M. Azizi, "Adaptive fractional order fast terminal dynamic sliding mode controller design for antilock braking system (ABS)," *Int. J. Dyn. Control*, vol. 7, no. 1, pp. 368–378, Mar. 2019.
[18] H. Mirzaeinejad and M. Mirzaei, "A novel method for non-linear control of wheel slip in anti-lock braking systems," *Control Eng. Pract.*, vol. 18, no. 8, pp. 918–926, Aug. 2010.
[19] S. Formentin, C. Novara, S. M. Savaresi, and M. Milanese, "Active braking control system design: The D^2-IBC approach," *IEEE/ASME Trans. Mechatronics*, vol. 20, no. 4, pp. 1573–1584, Apr. 2015.
[20] C. A. Lúa, S. Di Gennaro, and M. E. S. Morales, "Nonlinear adaptive controller applied to an antilock braking system with parameters variations," *Int. J. Control, Autom. Syst.*, vol. 15, no. 5, pp. 2043–2052, Oct. 2017.
[21] R. He and L. Yuan, "An improved nonlinear predictive control strategy enhanced by fractional order extremum seeking control of the antilock braking system of a vehicle," *IEEE Access*, vol. 8, pp. 168576–168588, 2020.
[22] A. Aksjonov, V. Ricciardi, K. Augsburg, V. Vodovozov, and E. Petlenkov, "Hardware-in-the-loop test of an open-loop fuzzy control method for decoupled electrohydraulic antilock braking system," *IEEE Trans. Fuzzy Syst.*, vol. 29, no. 5, pp. 965–975, May 2021.
[23] H. A. Abbas, A. Rabhi, and M. Belkheiri, "Adaptive intelligent control of the ABS nonlinear systems using RBF neural network based on K-means clustering," in *Proc. Int. Conf. Electron. Eng. Renew. Energy*. Singapore: Springer, 2020, pp. 503–512.
[24] X. Bu, "Air-breathing hypersonic vehicles funnel control using neural approximation of non-affine dynamics," *IEEE/ASME Trans. Mechatronics*, vol. 23, no. 5, pp. 2099–2108, Oct. 2018.
[25] X. Bu and Q. Qi, "Fuzzy optimal tracking control of hypersonic flight vehicles via single-network adaptive critic design," *IEEE Trans. Fuzzy Syst.*, vol. 30, no. 1, pp. 270–278, Jan. 2022.
[26] X. Bu, B. Jiang, and H. Lei, "Non-fragile quantitative prescribed performance control of waverider vehicles with actuator saturation," *IEEE Trans. Aerosp. Electron. Syst.*, early access, Feb. 25, 2022, doi: 10.1109/TAES.2022.3153429.
[27] X. Bu, Y. Xiao, and H. Lei, "An adaptive critic design-based fuzzy neural controller for hypersonic vehicles: Predefined behavioral nonaffine control," *IEEE/ASME Trans. Mechatron.*, vol. 24, no. 4, pp. 1871–1881, Jul. 2019.
[28] L. A. Zadeh, "The concept of a linguistic variable and its application to approximate reasoning-I," *Inf. Sci.*, vol. 8, no. 3, pp. 199–249, 1975.
[29] J. M. Mendel, R. I. John, and F. Liu, "Interval type-2 fuzzy logic systems made simple," *IEEE Trans. Fuzzy Syst.*, vol. 14, no. 6, pp. 808–821, Dec. 2006.
[30] M. Shirzadeh, A. Amirkhani, M. H. Shojaeefard, and H. Behroozi, "Adaptive fuzzy sliding mode and indirect radial-basis-function neural network controller for trajectory tracking control of a car-like robot," *Int. J. Nonlinear Anal. Appl.*, vol. 10, no. 1, pp. 153–166, 2019.
[31] O. Castillo and P. Melin, "A review on interval type-2 fuzzy logic applications in intelligent control," *Inf. Sci.*, vol. 279, pp. 615–631, Sep. 2014.
[32] M. A. Sanchez, O. Castillo, and J. R. Castro, "Generalized type-2 fuzzy systems for controlling a mobile robot and a performance comparison with interval type-2 and type-1 fuzzy systems," *Expert Syst. Appl.*, vol. 42, no. 14, pp. 5904–5914, Aug. 2015.
[33] A. Najafi, A. Amirkhani, K. Mohammadi, and A. Naimi, "A novel soft computing method based on interval type-2 fuzzy logic for classification of celiac disease," in *Proc. 23rd Iranian Conf. Biomed. Eng. 1st Int. Iranian Conf. Biomed. Eng. (ICBME)*, Tehran, Iran, 2016, pp. 257–262.
[34] Z. Lian, P. Shi, and C.-C. Lim, "Hybrid-triggered interval type-2 fuzzy control for networked systems under attacks," *Inf. Sci.*, vol. 567, pp. 332–347, Aug. 2021.
[35] S. H. Jana and B. Jana, "Application of random triangular and Gaussian type-2 fuzzy variable to solve fixed charge multi-item four dimensional transportation problem," *Appl. Soft Comput.*, vol. 96, Nov. 2020, Art. no. 106589.
[36] T. Wu, X. Liu, J. Qin, and F. Herrera, "An interval type-2 fuzzy Kano-prospect-TOPSIS based QFD model: Application to Chinese e-commerce service design," *Appl. Soft Comput.*, vol. 111, Nov. 2021, Art. no. 107665.
[37] M. Shirzadeh, A. Amirkhani, N. Tork, and H. Taghavifar, "Trajectory tracking of a quadrotor using a robust adaptive type-2 fuzzy neural controller optimized by cuckoo algorithm," *ISA Trans.*, vol. 114, pp. 171–190, Aug. 2021.
[38] J. A. Cabrera, A. Ortiz, J. J. Castillo, and A. Simon, "A fuzzy logic control for antilock braking system integrated in the IMMa tire test bench," *IEEE Trans. Veh. Technol.*, vol. 54, no. 6, pp. 1937–1949, Nov. 2005.
[39] A. B. Sharkawy, "Genetic fuzzy self-tuning PID controllers for antilock braking systems," *Eng. Appl. Artif. Intell.*, vol. 23, no. 7, pp. 1041–1052, Oct. 2010.
[40] J. P. Fernandez, M. A. Vargas, J. M. V. Garcia, J. A. C. Carrillo, and J. J. C. Aguilar, "Coevolutionary optimization of a fuzzy logic controller for antilock braking systems under changing road conditions," *IEEE Trans. Veh. Technol.*, vol. 70, no. 2, pp. 1255–1268, Feb. 2021.
[41] W. Bai, Q. Zhou, T. Li, and H. Li, "Adaptive reinforcement learning neural network control for uncertain nonlinear system with input saturation," *IEEE Trans. Cybern.*, vol. 50, no. 8, pp. 3433–3443, Aug. 2020.
[42] B. J. Pandian and M. M. Noel, "Control of constrained high dimensional nonlinear liquid level processes using a novel neural network based rapidly exploring random tree algorithm," *Appl. Soft Comput.*, vol. 96, Nov. 2020, Art. no. 106709.
[43] M. Shirzadeh, A. Amirkhani, A. Jalali, and M. R. Mosavi, "An indirect adaptive neural control of a visual-based quadrotor robot for pursuing a moving target," *ISA Trans.*, vol. 59, pp. 290–302, Nov. 2015.
[44] M. Shirzadeh, H. J. Asl, A. Amirkhani, and A. A. Jalali, "Vision-based control of a quadrotor utilizing artificial neural networks for tracking of moving targets," *Eng. Appl. Artif. Intell.*, vol. 58, pp. 34–48, Feb. 2017.
[45] A. Amirkhani, M. Shirzadeh, N. Tork, and S. B. Shokouhi, "Path tracking of an autonomous vehicle by means of an indirect adaptive neural controller," in *Proc. 7th Int. Conf. Robot. Mechatronics (ICRoM)*, Tehran, Iran, Nov. 2019, pp. 398–403.
[46] A. Amirkhani, M. Shirzadeh, M. H. Shojaeefard, and A. Abraham, "Controlling wheeled mobile robot considering the effects of uncertainty with neuro-fuzzy cognitive map," *ISA Trans.*, vol. 100, pp. 454–468, May 2020.
[47] R. J. Kuo and F. E. Zulvia, "The application of gradient evolution algorithm to an intuitionistic fuzzy neural network for forecasting medical cost of acute hepatitis treatment in Taiwan," *Appl. Soft Comput.*, vol. 111, Nov. 2021, Art. no. 107711.
[48] L. Jinkun and X. Wang, *Advanced Sliding Mode Control for Mechanical Systems*. Berlin, Germany: Springer, 2012.
[49] H. Wang, S. Wu, and Q. Wang, "Global sliding mode control for nonlinear vehicle antilock braking system," *IEEE Access*, vol. 9, pp. 40349–40359, 2021.
[50] J.-J. E. Slotine and W. Li, *Applied Nonlinear Control*. Englewood Cliffs, NJ, USA: Prentice-Hall, 1991.
[51] M. Shirzadeh, M. H. Shojaeefard, A. Amirkhani, and H. Behroozi, "Adaptive fuzzy nonlinear sliding-mode controller for a car-like robot," in *Proc. 5th Conf. Knowl. Based Eng. Innov. (KBEI)*, Tehran, Iran, Feb. 2019, pp. 686–691.
[52] J. Guo, X. Jian, and G. Lin, "Performance evaluation of an anti-lock braking system for electric vehicles with a fuzzy sliding mode controller," *Energies*, vol. 7, no. 10, pp. 6459–6476, 2014.
[53] A. M. Boopathi and A. Abudhahir, "Adaptive fuzzy sliding mode controller for wheel slip control in antilock braking system," *J. Eng. Res.*, vol. 4, no. 2, pp. 1–19, Apr. 2016.
[54] S. Saremi, S. Mirjalili, and A. Lewis, "Grasshopper optimisation algorithm: Theory and application," *Adv. Eng. Softw.*, vol. 105, pp. 30–47, Mar. 2017.

[55] Y. Meraihi, A. B. Gabis, S. Mirjalili, and A. Ramdane-Cherif, "Grasshopper optimization algorithm: Theory, variants, and applications," *IEEE Access*, vol. 9, pp. 50001–50024, 2021.
[56] M. Garziad and A. Saka, "Towards a comparative assessment between physical and characteristic of tire of two-wheeler vehicle," in *Proc. Int. Conf. Integr. Design Production*. Cham, Switzerland: Springer, 2019, pp. 161–177.
[57] J. M. Mendel, "Uncertain rule-based fuzzy systems," in *Type-2 Fuzzy Sets*. Cham, Switzerland: Springer, 2017, pp. 259–306.
[58] A. Amirkhani, M. Shirzadeh, T. Kumbasar, and B. Mashadi, "A framework for designing cognitive trajectory controllers using genetically evolved interval type-2 fuzzy cognitive maps," *Int. J. Intell. Syst.*, vol. 37, no. 1, pp. 305–335, Jan. 2022.
[59] D. Wu and J. M. Mendel, "Enhanced Karnik–Mendel algorithms," *IEEE Trans. Fuzzy Syst.*, vol. 17, no. 4, pp. 923–934, Aug. 2008.
[60] A. Amirkhani, M. Shirzadeh, and T. Kumbasar, "Interval type-2 fuzzy cognitive map-based flight control system for quadcopters," *Int. J. Fuzzy Syst.*, vol. 22, no. 8, pp. 2504–2520, Nov. 2020.
[61] J. Liu, *Intelligent Control Design and MATLAB Simulation*. Singapore: Springer, 2018.

ABDOLLAH AMIRKHANI (Senior Member, IEEE) received the M.Sc. and Ph.D. degrees (Hons.) in electrical engineering from the Iran University of Science and Technology (IUST), Tehran, in 2012 and 2017, respectively. He is currently an Assistant Professor with the School of Automotive Engineering, IUST. He has been actively involved in several national research and development projects, related to the development of new methodologies and learning algorithms based on AI techniques. His research interests include machine vision, fuzzy cognitive maps, data mining, and machine learning. He received the Outstanding Student Award from the First Vice President of Iran, in 2015. In 2016, he was Conferred Award by the Ministry of Science, Research and Technology. He is an Associate Editor of the *Engineering Science and Technology, an International Journal*.

MASOUD SHIRZADEH (Member, IEEE) received the M.Sc. degree in control engineering from the Iran University of Science and Technology (IUST), in 2015, and the M.Sc. degree (Hons.) in mechatronics engineering from the Amirkabir University of Technology (AUT), Tehran, Iran, in 2019. His research interests include soft computing, intelligent control, mechatronics, robotics, and fuzzy theory.

MAHDI MOLAIE received the B.Sc. degree in electrical engineering from the University of Mazandaran. He is currently pursuing the master's degree in digital electronics with the Iran University of Science and Technology (IUST), Tehran, Iran. His research interests include autonomous vehicles, type-2 fuzzy sets and systems, intelligent systems, deep learning, and machine learning.